# Thermal hybrid exchange-correlation density functional for improving the description of warm dense matter

D. I. Mihaylov [*], V. V. Karasiev,[†] and S. X. Hu

*Laboratory for Laser Energetics, University of Rochester, 250 East River Road, Rochester, New York 14623-1299, USA*

Finite-temperature density functional theory has become a standard tool for first-principles calculations of the properties of warm dense matter (WDM) relevant to high-energy-density physics (HEDP) applications. Here we present theoretical grounds of thermal hybrid exchange-correlation (XC) functionals within the generalized Mermin-Kohn-Sham scheme for an improved description of WDM. Building on the previously developed KSDT (Karasiev-Sjostrom-Dufty-Trickey) [Karasiev *et al.*, Phys. Rev. Lett. **112**, 076403 (2014)] local density approximation (LDA) and the KDT16 (Karasiev-Dufty-Trickey 2016) [Karasiev *et al.*, Phys. Rev. Lett. **120**, 076401 (2018)] generalized-gradient approximation (GGA) XC *free-energy* density functionals, we construct a novel thermal hybrid XC functional, referred to here as KDT0. The KDT0 model at low temperature reduces to the popular ground-state PBE0 hybrid due to properties of the used KDT16 density functional approximation. Application to static calculations of electronic band gap and band structure at a wide range of temperatures for various systems of interest to HEDP show that KDT0 provides a significant improvement to the lower LDA and GGA rung XC functionals and to the ground-state PBE0 hybrid.

## I. INTRODUCTION

Understanding warm dense matter (WDM) characterized by elevated temperature ($\sim 10^3$–$10^7$ K) and a wide range of densities ($\sim 10^{-1}$–$10^5$ g/cm$^3$) is essential to high-energy-density physics (HEDP). It poses challenges to both experimental and theoretical efforts in fields such as inertial confinement fusion, plasma physics, and planetary science [1–10]. From the theoretical point of view, the WDM regime is too hot for standard condensed matter approaches; however, quantum many-body effects are strong and classical plasma physics is not applicable. An established, standard approach for accurate treatment of WDM is *ab initio* molecular dynamics (AIMD), when classical treatment for ions is combined with finite-temperature density functional theory (FT-DFT) for electronic degrees of freedom [11–18].

The biggest source of error in FT-DFT-based molecular dynamics is the use of an approximate XC density functional, the choice of which is usually guided by the desired level of accuracy and computational cost requirements [19]. Regardless of choice, to the best of the authors' knowledge, with one exception [20,21], all available XC functionals in commonly used DFT software packages are ground-state functionals which do not explicitly depend on $T$, but are evaluated at the $T$-dependent self-consistent density, i.e., $\mathcal{F}_{xc}[n(T), T] \approx E_{xc}[n(T)]$—an approach known as the ground-state approximation (GSA) [22,23]. The exception is the PROFESS@QUANTUM-ESPRESSO package, which

implements KSDT thermal LDA XC. In order to clearly distinguish between the two DFT approaches, those utilizing $\mathcal{F}_{xc}[n(T), T]$ will be referred to as "finite-temperature approximation" (FTA) or "thermal" and those utilizing $E_{xc}[n(T)]$ as "GSA." Also, for compactness, the phrase "free-energy-density XC functionals with explicit $T$ dependence" will be substituted with "thermal XC functionals."

Previously developed thermal functionals belong to the LDA and GGA level of refinement. At the LDA level Karasiev *et al.* developed the nonempirical, thermal functional KSDT [20] (and its corrected version—corrKSDT; see Supplemental Material in Ref. [24]), which is based on parametrized path-integral Monte Carlo (PIMC) data for the homogeneous electron gas (HEG) at finite $T$ [25,26] and, in the zero-$T$ limit, reduces to the ground-state Perdew-Zunger (PZ) functional [27]. Groth *et al.* [28] used the KSDT approach and protocol to reparametrize the HEG XC free-energy resulting in representation denoted as "GDSMFB". The equivalence of these two representations, GDSMFB and corrKSDT, was recently demonstrated [29].

Subsequently, driven by the need to incorporate density gradient effects and thereby account for the nonhomogeneity of the system [30–32], Karasiev *et al.* developed the GGA-level thermal functional KDT16 [24] by analyzing the gradient expansion of weakly inhomogeneous electron gas at finite-$T$ and defining appropriate $T$-dependent reduced variables for X and C. KDT16 is, by construction, nonempirical and reduces to the popular Perdew-Burke-Ernzerhof (PBE) functional [33] in the zero-$T$ limit. An example of the improved accuracy provided by the KDT16 functional was recently reported in Ref. [34], where KDT16-based AIMD studies of shocked deuterium showed improved agreement

---

*dmih@lle.rochester.edu

†Corresponding author: vkarasev@lle.rochester.edu

with experimental measurements of Hugoniot, reflectivity, and dc conductivity at elevated $T$.

While it is clear that corrKSDT and KDT16 provide an apparent improvement on their ground-state counterparts, PZ and PBE, they suffer from an inherent fundamental drawback—underestimating the electronic band gap, $E_{\text{gap}}$ [35]. This is not a drawback associated with the PZ and PBE functionals alone, but with KS DFT multiplicative potential in general and improving the description of the electronic gap is the main reason for the development of density functionals beyond the GGA, such as meta-GGAs and hybrids, an approach that includes a nonlocal potential operator and is known as the generalized Kohn-Sham (GKS) theory [36]. Hybrid XC functionals, such as PBE0 [37,38] and HSE [39], are constructed by mixing DFT XC functionals with Hartree-Fock (HF) exact exchange (EXX) and are known to be superior to GGAs in predicting quantities such as $E_{\text{gap}}$, atomization energy, bond length, and vibrational frequency, with HSE generally showing better agreement with experiment [36,40,41]. However, PBE0 and HSE are both ground state and a thermal XC functional at the hybrid level of DFT is yet to be developed. Recently, an advanced thermal XC functional with exact treatment of the X interaction was presented, although not within the Kohn-Sham DFT, but within the reduced-density-matrix functional theory formalism [42,43]. In this article we remedy that deficiency by providing theoretical grounds for thermal hybrid functionals and presenting the KDT0 thermal hybrid model which is based on a mixture of finite-$T$ HF X and thermal KDT16 GGA XC. This thermal hybrid at low-$T$ reduces to the popular ground-state PBE0. As we show here, hybrid functionals with admixture of thermal HF X predict the qualitatively correct behavior for $E_{\text{gap}}$ as a function of electronic temperature $T$ (calculated at fixed ionic configuration)—$E_{\text{gap}}(T)$ decreases as $T$ rises. This is in contrast to the LDA/GGA rung functionals, which tend to predict a monotonically increasing $E_{\text{gap}}(T)$. This results from the fact that the HF approximation can be generalized to finite $T$; therefore, HF EXX naturally includes the exact $T$ dependence of the X term [12,44]. Recent work [31] found significant qualitative differences in X free energy and pressure between the ground-state and thermal DFT and the finite-$T$ HF approaches.

## II. THEORETICAL GROUNDS OF THERMAL HYBRID XC FUNCTIONALS

The main goal of our work here is to develop a novel thermal hybrid XC functional, which provides an improved accuracy in calculations of $E_{\text{gap}}(T)$ for a wide range of $T$. XC free energy [see Eq. (2) in Ref. [20] for definition] could be partitioned into exchange (X) and correlation (C). In the zero-$T$ case the single-determinant X energy could be defined within the HF and EXX Kohn-Sham methods. The EXX energy formalism developed within the Kohn-Sham DFT [45,46] formally uses the HF expression for X, but the X potential is a local multiplicative operator, as opposed to the nonlocal HF X operator. The two methods, HF and EXX, provide very close values for X energy and energy of occupied orbitals, whereas virtual (unoccupied) orbital energies obtained from EXX are significantly lower as compared to

the HF values. The thermal generalization of the zero-$T$ HF single-Slater determinant X may be expressed in terms of a one-electron reduced density matrix (1-RDM) (see Ref. [47]) and leads to the following definition of thermal HF X:

$$\mathcal{F}_{\text{x}}^{\text{HF}}[n, T] := -\int d\mathbf{x}_1 \, d\mathbf{x}_2 \left\{ \frac{1}{2} g_{12} \bar{\Gamma}^{(1)}(\mathbf{x}_1|\mathbf{x}_2'; T) \right.$$
$$\left. \times \bar{\Gamma}^{(1)}(\mathbf{x}_2|\mathbf{x}_1'; T) \right\}_{\mathbf{x}_1' = \mathbf{x}_1, \mathbf{x}_2' = \mathbf{x}_2}, \quad (1)$$

where $\mathbf{x} := \mathbf{r}, s$ is a composite space-spin variable, $g_{12} = 1/|\mathbf{r}_1 - \mathbf{r}_2|$, and the 1-RDM is defined in terms of the MKS orbitals and Fermi-Dirac occupation numbers, $f_i(T) = [1 + \exp(\frac{\varepsilon_i - \mu}{k_B T})]^{-1}$ ($\mu$ being the chemical potential and $\varepsilon_i$ are MKS eigenvalues), as

$$\bar{\Gamma}^{(1)}(\mathbf{x}_1|\mathbf{x}_1'; T) := \sum_{j=1}^{\infty} f_j(T) \phi_j(\mathbf{x}_1) \phi_j^*(\mathbf{x}_1'). \quad (2)$$

The analog of thermal HF is called finite-temperature (ft) EXX DFT [48]. As in the zero-$T$ case, ftEXX defines the exchange free-energy formally identically with HF, but follows a true MKS procedure with a local (multiplicative) exchange potential followed from the system response function. Hereinafter we will discuss the thermal HF exchange within the generalized Mermin-Kohn-Sham (MKS) formalism, when the corresponding X potential (or its fraction) is represented by a nonlocal exchange operator of the HF form with use of generalized MKS one-electron states for evaluation of the exchange energy and exchange operator.

The thermal adiabatic connection formula derived in Ref. [49], $\mathcal{F}_{\text{xc}}[n, T] = \int_0^1 d\lambda \, \mathcal{U}_{\text{xc},\lambda}[n, T]$, provides theoretical grounds to develop thermal hybrid functionals. The integrand in the above in-line equation is the difference between the electron–electron interaction potential energy of the interacting system (with the electron-electron interaction operator scaled by a coupling constant $\lambda$, $\mathcal{V}_{\text{ee},\lambda}[n, T]$) and the Hartree energy: $\mathcal{U}_{\text{xc},\lambda}[n, T] = \mathcal{V}_{\text{ee},\lambda}[n, T] - \mathcal{F}_{\text{H}}[n]$. A simple two-point approximation to the integral leads to $\mathcal{F}_{\text{xc}}[n, T] \approx (1/2)(\mathcal{U}_{\text{xc},\lambda=1}[n, T] + \mathcal{U}_{\text{xc},\lambda=0}[n, T])$, where the energy difference $\mathcal{U}_{\text{xc},\lambda=0}$ for the noninteracting MKS system is equal to the HF X free energy, $\mathcal{F}_{\text{x}}^{\text{HF}}[n, T] = \mathcal{U}_{\text{xc},\lambda=0}[n, T] \equiv \mathcal{V}_{\text{ee},\lambda=0}[n, T] - \mathcal{F}_{\text{H}}[n]$, and the first term, $(1/2)\mathcal{U}_{\text{xc},\lambda=1}[n, T]$, which, in a way similar to the ground-state case [50], can be approximated by a suitable XC *free-energy* density functional approximation (DFA), $(1/2)\mathcal{U}_{\text{xc},\lambda=1} \approx (1/2)\mathcal{F}_{\text{x}}^{\text{DFA}} + \mathcal{F}_{\text{c}}^{\text{DFA}}$, such that $\mathcal{F}_{\text{xc}}[n, T] \approx (1/2)\mathcal{F}_{\text{x}}^{\text{HF}} + (1/2)\mathcal{F}_{\text{x}}^{\text{DFA}} + \mathcal{F}_{\text{c}}^{\text{DFA}}$. Generalization of the above two-point approximation leads to a simple one-parameter hybrid XC *free-energy* functional

$$\mathcal{F}_{\text{xc}}^{\text{hyb}}[n, T] = \mathcal{F}_{\text{xc}}^{\text{DFA}}[n, T] + a(\mathcal{F}_{\text{x}}^{\text{HF}}[n, T] - \mathcal{F}_{\text{x}}^{\text{DFA}}[n, T]). \quad (3)$$

The value of $a = 1/4$, rationalized in Ref. [37] for the ground-state case, will provide a consistent zero-$T$ limit of Eq. (3). Dependence of $a$ on $T$ is a matter of future investigation. Employment of the most advanced (up to date) KDT16 GGA XC in Eq. (3), namely $\mathcal{F}_{\text{xc}}^{\text{DFA}} = \mathcal{F}_{\text{xc}}^{\text{KDT16}}$ and $\mathcal{F}_{\text{x}}^{\text{DFA}} = \mathcal{F}_{\text{x}}^{\text{KDT16}}$, leads to the KDT0 thermal hybrid functional discussed in this paper. In the zero-$T$ limit the KDT0 model reduces to the PBE0 ground-state hybrid due to the KDT16 free-energy reducing to the PBE ground-state XC, which has been

demonstrated in Ref. [24] and is the case for all $E_{\text{gap}}(T)$ calculations performed here. Proper temperature scaling in KDT0 is ensured through the correctly scaled KDT16 [24,49].

## III. COMPUTATIONAL DETAILS

In order to compare performance between KDT0 and PBE0 we perform static calculations of band gap as a function of electronic temperature $E_{\text{gap}}(T)$ when positions of ions are fixed at near-ambient conditions. This corresponds to a two-temperature model, cold ions $T_{\text{ion}} \approx 0$ K, and $T$ is the temperature of electrons $T_e = T$. This model is relevant to HED experiments such as ultrafast femtosecond laser heating of materials [51] or isochoric heating via ultrafast proton beams [52] in which hot electrons are produced while the lattice is still cold. Full $E_{\text{gap}}$ dependence on $T$ is determined by allowing the ions to move according to forces calculated at every electronic step (AIMD simulation); however, such calculations with hybrid-level functionals are computationally expensive and unnecessary for the purpose of introducing and testing the hybrid *free-energy* density functional presented here. We also perform band structure calculations at low- and high-$T$ to investigate the effect of KDT0 on valence and conduction band orbitals within the Brillouin zone (BZ). The systems of choice are Si, C, $CH_4$, polystyrene (CH), and $H_2O$. The choice of Si and C was motivated by the need to compare the KDT0 functional to the highly accurate finite-$T$ *GW* [53] calculations. We also perform calculations for CH, $CH_4$, and $H_2O$, which are of relevance to HEDP experiments and planetary science where thermal functionals could provide an improvement to, e.g., equation-of-state calculations. In addition, calculations on $CH_4$ and $H_2O$ allow us to study the effect of KDT0 on systems with a relatively large low-$T$ band gap.

All calculations were performed with the Vienna *ab initio* simulation package (VASP) [54,55], which implements the projector-augmented wave (PAW) method [56,57]. The KDT16 functional was implemented in a locally modified version of the software. KDT0, which comes at the same computational cost as PBE0, was then constructed from KDT16 and thermal HF X, which is readily available in VASP. For all systems, except CH, atomic coordinates and cell parameters were extracted from Ref. [58] and the reported experimental lattice constants were used.

Here, it is important to note that PBE0, as implemented in VASP, is constructed from thermal HF X $\mathcal{F}_x^{\text{HF}}[n, T]$ [see Eqs. (1) and (2)] and ground-state PBE XC. This differs from the true ground-state PBE0 as introduced in Ref. [37], where HF X is by definition ground state, i.e., $E_x^{\text{HF}}[n]$. Therefore, what is considered ground-state PBE0 in the work presented here refers to PBE0 constructed from ($T$-independent) ground-state PBE XC and thermal HF X. Although this is not the true ground-state PBE0, it serves as a convenient measure of the XC thermal effects provided by KDT0 through the finite-$T$ GGA KDT16.

For all hybrid functional calculations we use a relatively dense **k** mesh for which we employ **k** point parallelism [59], which is implemented in VASP and allows for simultaneous parallelism over **k** points and bands and is necessary for high-$T$ calculations, where the number of contributing bands

grows significantly due to Fermi-Dirac (FD) thermal occupations. All bands with occupation greater than $10^{-7}$ were included. $E_{\text{gap}}$ at all $T$ is defined as the energy difference between what is the lowest unoccupied molecular orbital (LUMO) and the highest occupied molecular orbital (HOMO) at the zero-$T$ limit. For the $T$ ranges considered here this definition is still valid even though LUMO becomes partially occupied and HOMO partially unoccupied. An equivalent unambiguous definition we introduce here is the following: $E_{\text{gap}} = \min_{\mathbf{k}}\{\varepsilon_{N+1,\mathbf{k}}\} - \max_{\mathbf{k}}\{\varepsilon_{N,\mathbf{k}}\}$, where $N$ is the number of electrons in the system and $\varepsilon_{i,\mathbf{k}}$ are band energies and we assume $0 \leqslant f_{i,\mathbf{k}} \leqslant 1$ for occupations. With BZ sampling this definition of $E_{\text{gap}}$ corresponds to the energy difference between the conduction $N + 1$ band minimum and the valence $N$ band maximum.

For diamond, Si, and $CH_4$, the BZ was sampled using a $15 \times 15 \times 15$ Monkhorst-Pack **k** mesh. $H_2O$ calculations were performed with a $7 \times 7 \times 7$ and CH with a $3 \times 3 \times 8$ **k** mesh. CH was simulated with a box containing two styrene ($C_8H_8$) monomers that were oriented with respect to each other so that the (periodic) syndiotactic CH polymer chain is built according to Refs. [60,61]. Our atomistic model of CH predicts $E_{\text{gap}} = 2.92$ eV with PBE and $E_{\text{gap}} = 4.53$ eV with PBE0, which are within the expected range of values predicted by those functionals considering the reported experimental value of 4.14 eV [62] and a high-precision *GW* estimation of 4.4 eV [63]. For band-structure calculations of Si (cubic diamond [64]) and $CH_4$ (fcc [65]) at each of the three selected temperatures, a $20 \times 20 \times 20$ $\Gamma$-centered **k** mesh was used, which produced 11 points along the symmetry paths $L$-$\Gamma$ and $\Gamma$-$X$.

## IV. RESULTS AND DISCUSSION

In order to validate any improved performance provided by hybrid-level functionals, we shall refer to high-precision first-principles many-body perturbation theory approaches that have been reported to achieve excellent agreement with experiment. Recent theoretical studies of $E_{\text{gap}}$ in various semiconductors at low-$T$ based on DFT and *GW* showed that the quasiparticle self-consistent *GW* (QS*GW*) method achieves much better agreement with experiment than LDA or GGA ground-state functionals, which are known to significantly underestimate the $E_{\text{gap}}(T)$ [66]. Consequently, Faleev *et al.* extended their theory to include finite-$T$ effects (FT QPSC*GW*) and published results for $E_{\text{gap}}(T)$ for several widely used semiconductors for $T$ up to 47 kK (GaAs, Si, Ge, InSb) and 140 kK (diamond) [53].

Experimental measurements for $E_{\text{gap}}(T)$ while holding contributions to $E_{\text{gap}}(T)$ due to thermal motion of ions low are difficult to obtain, although pump-probe measurements [67,68] show a decrease in the gap in the subpicosecond regime during which electrons are much hotter than the lattice, in agreement with FT QPSC*GW*, referred to as FT *GW* hereafter. One of the main conclusions reached in Ref. [53] is that at high-$T$ the use of LDA within the GSA (e.g., in large-scale AIMD simulations) can be justified since there is little difference in band structure between it and FT *GW*— a conclusion based on results that are largely due to error cancellation as the ground-state LDA underestimates $E_{\text{gap}}$ at
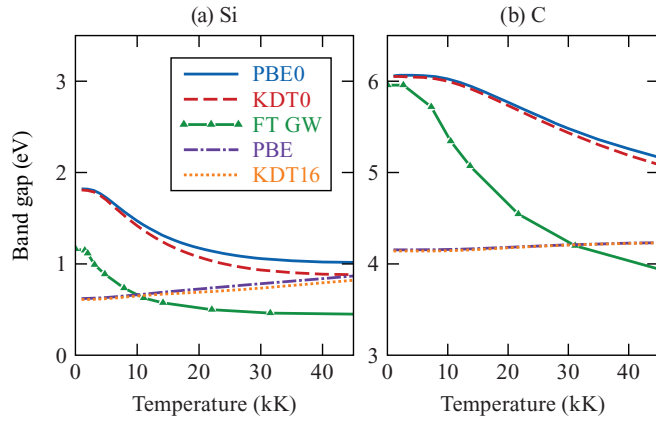
FIG. 1. Band gaps of (a) Si and (b) diamond (C) as a function of electronic temperature calculated with ground-state PBE and PBE0 and thermal KDT16 and KDT0 functionals. The green curve (FT GW) was extracted from Ref. [53].

low $T$ and then, contrary to FT $GW$, predicts a universally increasing $E_{gap}(T)$ with rising $T$. Such error cancellations, however, have a limited scope of reliability since they only occur in $T$ ranges that are strongly system dependent and often very limited.

Figure 1 shows $E_{gap}(T)$ results for Si and diamond, which are two of the systems addressed in Ref. [53]. Let us first compare the GSA functionals PBE and PBE0 in the case of Si. At low $T$ they both give an approximately equally wrong value for the $E_{gap}$, with PBE underestimating it and PBE0 overestimating it. At higher $T$ PBE0 predicts the same qualitative behavior as FT $GW$—monotonically decreasing $E_{gap}(T)$—while PBE predicts a monotonically increasing $E_{gap}(T)$, which is in direct contrast with FT $GW$ predictions. The correct qualitative trend for $E_{gap}(T)$ predicted by PBE0 is a direct result of including $T$ effects in XC through the $T$-dependent HF X and serves as an indication of the importance of thermal effects in XC. The same improvement in the qualitative behavior of $E_{gap}(T)$ provided by PBE0 is seen in diamond [Fig. 1(b)].

Next, we turn our attention to results obtained with the thermal functionals KDT16 and KDT0. Most importantly, in both systems thermal XC effects lower the $E_{gap}(T)$ curve toward the more-accurate FT $GW$ results, thereby improving qualitative behavior for all temperatures considered. However, we stress two important observations: (i) the thermal corrections are strongly system dependent, with the relative difference in the gaps predicted by PBE0 and KDT0 reaching a maximum of 12.7 % in Si and only 1.5 % in diamond at $T = 45$ kK (see Fig. 3) and (ii) $\Delta E_{gap}(T)$ for hybrid-level functionals is larger than that for GGAs, which is a result of the different treatment of thermal effects in the X interaction between the hybrid and GGA levels of approximation. Note that the corrections provided by KDT0 at higher $T$ correspond to the magnitude of the XC thermal effects and the fact that $E_{gap}(T)$ is still significantly overestimated is a drawback inherited from PBE0.

Motivated by these observations, we apply KDT0 and KDT16 to other systems of drastically different properties, such as density $\rho$ and $E_{gap}$ at near-ambient conditions. Results
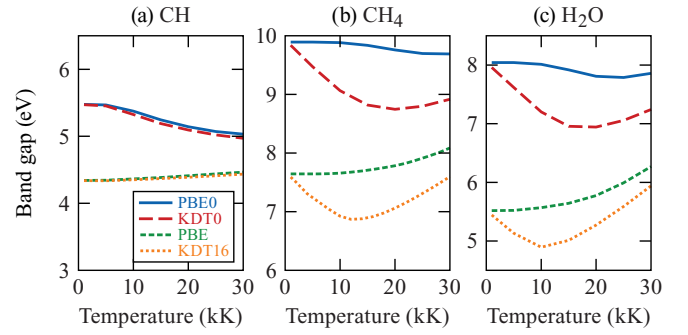


FIG. 2. Band gaps as a function of electronic temperature calculated with thermal (KDT0 and KDT16) and ground-state (PBE0 and PBE) functionals.

for $E_{gap}(T)$ in CH, CH$_4$, and H$_2$O for $T$ up to 30 kK are shown in Fig. 2.

In CH, $\rho = 1.06$ g/cm$^3$, relative differences in $E_{gap}(T)$ predicted by PBE0 and KDT0 (see Fig. 3) are small ($<2.5\%$) and comparable to those in diamond. For CH$_4$, $\rho = 0.43$ g/cm$^3$, and H$_2$O, $\rho = 0.96$ g/cm$^3$, $\Delta E_{gap}(T)$ reaches values comparable to those in Si at 45 kK, although the peaks occur at much lower $T$. This suggests that the temperature range in which XC thermal corrections to $E_{gap}$ are most prominent is also strongly system dependent. This observation is consistent with the behavior of relative thermal XC corrections for the HEG as a function of $T$ and density, when thermal XC corrections become important in the range of reduced temperature between 0.3 and 1 (see Fig. 2 and corresponding discussion in Ref. [30]). At high $T$ the trend for $E_{gap}(T)$ is reversed, (see, e.g., H$_2$O at $T > 20$ kK) and according to both PBE0 and KDT0 the gap starts increasing.
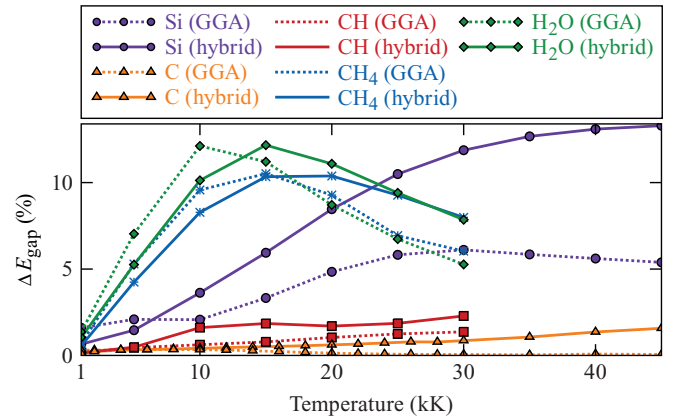


FIG. 3. Relative difference between $E_{gap}(T)$ predicted by GSA and thermal XC: $[(E_{gap}^{\text{GSA-XC}} - E_{gap}^{\text{thermal-XC}})/(E_{gap}^{\text{GSA-XC}})] \times 100$, where GSA-XC refers to PBE/PBE0 in case of (GGA)/(Hyb.) and thermal-XC refers to KDT16/KDT0 in case (GGA)/(Hyb.). Dotted lines correspond to GGA-level and solid lines correspond to hybrid-level thermal corrections. Colors correspond to different systems, the absolute values of the gaps for which are shown in Figs. 1 and 2. For example, the solid purple line represents the relative difference in $E_{gap}(T)$ predicted by hybrid-level functionals PBE0 and KDT0, i.e., $\Delta E_{gap}^{\text{hybrid}}(T) = \{[E_{gap}^{\text{PBE0}}(T) - E_{gap}^{\text{KDT0}}(T)]/[E_{gap}^{\text{PBE0}}(T)]\} \times 100$.
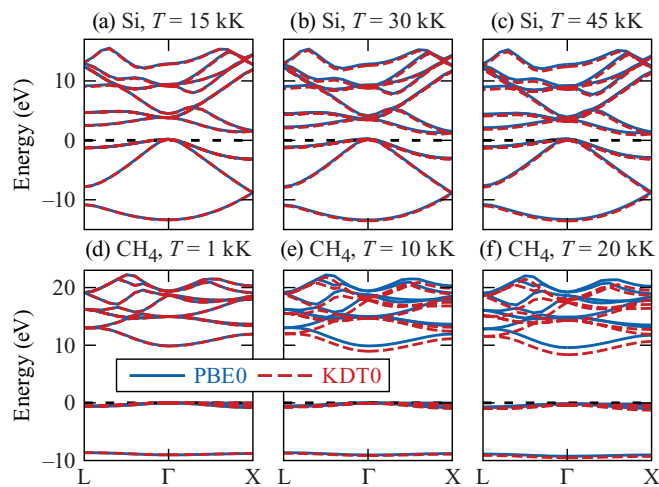
FIG. 4. Band structure of Si (top row, 15, 30, and 45 kK) and CH$_4$ (bottom row, 1, 10, and 20 kK). The valence band maximum in the lowest-$T$ case (15 kK in the case of Si and 1 kK in the case of CH$_4$) has been shifted to $E = 0$ eV (black, dashed line) and the same shift has been applied to the band diagrams in the corresponding higher-$T$ calculations to help visualize any lowering of the valence band states.

As seen in Fig. 3 for CH$_4$ and H$_2$O, the relative difference in $E_{\mathrm{gap}}(T)$ between KDT0 and PBE0 decreases at high $T$. For Si at 45 kK $\Delta E_{\mathrm{gap}}(T)$ starts to level off and although calculations at higher $T$ have not been performed, based on the decrease in $\Delta E_{\mathrm{gap}}(T)$ above 30 kK due to GGAs, it is expected that it too will decrease. This is because at the high-$T$ limit, which is correctly satisfied by KDT0, XC effects, and therefore XC thermal corrections, become negligible [29,30].

Results from band structure calculations at selected temperatures with PBE0 and KDT0 for Si [Figs. 4(a)–4(c)] and CH$_4$ [Figs. 4(d)–4(f)] show that the $E_{\mathrm{gap}}$ corrections due to KDT0 come primarily from correcting the overestimation of the conduction band state energies. In Si at $T = 45$ kK, the lowest three conduction bands, with both KDT0 and PBE0, are nearly degenerate at $\Gamma$ point and KDT0 predicts a 0.25 eV lowering from their PBE0 values—a 7.1% relative correction. The eighth highest conduction band appears at 0.38 eV lower energy with KDT0 than with PBE0—a 3.0% relative correction. For CH$_4$ at 20 kK [Fig. 4(f)] a similar trend, but with larger relative correction is observed—the lowest conduction band is lowered by KDT0 by 14.6%, while the eighth highest is lowered by 7.6%.

## V. CONCLUSIONS

Theoretical grounds of thermal hybrid XC functionals have been presented. Use of the KDT16 GGA XC free-energy density functional as density functional approximation for the exchange and correlation *free-energy* terms in the proposed model leads to the KDT0 thermal hybrid. Results for $E_{\mathrm{gap}}(T)$ in various systems of interest to HEDP show that KDT0 could provide a significant improvement to calculations of electronic properties at temperatures within the WDM regime. There are significant thermal XC effects on the entire band structure of studied systems, meaning that the accuracy of optic properties calculated via the Kubo-Greenwood formalism [69,70] depends on accounting for those effects via thermal hybrid XC functionals. Also, we show that the importance of XC thermal effects depends strongly on the type of system and $T$ range. In addition, we show that taking XC thermal effects into account at the hybrid level of approximation can lead to larger corrections compared to those at the GGA level of approximation and although KDT0 takes those effects into account, it still suffers from the fundamental drawback inherent through the PBE0 functional—significantly overestimating the gap. Therefore, KDT0 also serves as a justification for the need for further development of advanced thermal *free-energy* density functionals.

[1] R. S. Craxton, K. S. Anderson, T. R. Boehly, V. N. Goncharov, D. R. Harding, J. P. Knauer, R. L. McCrory, P. W. McKenty, D. D. Meyerhofer, and J. F. Myatt, Phys. Plasmas **22**, 110501 (2015).

[2] J. D. Lindl, R. L. McCrory, and E. M. Campbell, Phys. Today **45**(9), 32 (1992).

[3] M. D. Knudson and M. P. Desjarlais, Phys. Rev. Lett. **103**, 225501 (2009).

[4] M. D. Knudson, M. P. Desjarlais, A. Becker, R. W. Lemke, K. R. Cochrane, M. E. Savage, D. E. Bliss, T. R. Mattsson, and R. Redmer, Science **348**, 1455 (2015).

[5] H. R. Rüter and R. Redmer, Phys. Rev. Lett. **112**, 145007 (2014).

[6] F. Graziani, M. P. Desjarlais, R. Redmer, and S. B. Trickey, *Frontiers and Challenges in Warm Dense Matter* (Springer Science & Business, New York, 2014), Vol. 96.

[7] B. B. L. Witte, L. B. Fletcher, E. Galtier, E. Gamboa, H. J. Lee, U. Zastrau, R. Redmer, S. H. Glenzer, and P. Sperling, Phys. Rev. Lett. **118**, 225001 (2017).

[8] S. M. Vinko, O. Ciricosta, and J. S. Wark, Nat. Commun. **5**, 3533 (2014).

[9] S. X. Hu, Phys. Rev. Lett. **119**, 065001 (2017).

[10] S. X. Hu, B. Militzer, V. N. Goncharov, and S. Skupsky, Phys. Rev. Lett. **104**, 235003 (2010).

[11] W. Kohn and L. J. Sham, Phys. Rev. **140**, A1133 (1965).

[12] N. D. Mermin, Phys. Rev. **137**, A1441 (1965).

[13] M. V. Stoitsov and I. Z. Petkov, Ann. Phys. (NY) **184**, 121 (1988).

[14] R. Car and M. Parrinello, Phys. Rev. Lett. **55**, 2471 (1985).

[15] R. N. Barnett and U. Landman, Phys. Rev. B **48**, 2081 (1993).

[16] D. Marx and J. Hutter, in *Modern Methods and Algorithms of Quantum Chemistry*, 2nd ed., edited by J.Grotendorst, NIC Series Vol. 3 (John von Neumann Institute for Computing, Jülich, 2000), p. 329, and references therein.

[17] D. Marx and J. Hutter, *Ab-initio Molecular Dynamics: Basic Theory and Advanced Methods* (Cambridge University Press, Cambridge, UK, 2009).

[18] J. S. Tse, Annu. Rev. Phys. Chem. **53**, 249 (2002).

[19] J. P. Perdew and K. Schmidt, *Jacob's Ladder of Density Functional Approximations for the Exchange-Correlation Energy*, AIP Conf. Proc. No. 577 (American Institute of Physics, Melville, NY, 2001), pp. 1–20.

[20] V. V. Karasiev, T. Sjostrom, J. Dufty, and S. B. Trickey, Phys. Rev. Lett. **112**, 076403 (2014).

[21] V. V. Karasiev, T. Sjostrom, and S. B. Trickey, Comput. Phys. Commun. **185**, 3240 (2014).

[22] K. Burke, J. C. Smith, P. E. Grabowski, and A. Pribram-Jones, Phys. Rev. B **93**, 195132 (2016).

[23] J. C. Smith, A. Pribram-Jones, and K. Burke, Phys. Rev. B **93**, 245131 (2016).

[24] V. V. Karasiev, J. W. Dufty, and S. B. Trickey, Phys. Rev. Lett. **120**, 076401 (2018).

[25] E. W. Brown, B. K. Clark, J. L. DuBois, and D. M. Ceperley, Phys. Rev. Lett. **110**, 146405 (2013).

[26] T. Dornheim, S. Groth, T. Sjostrom, F. D. Malone, W. M. C. Foulkes, and M. Bonitz, Phys. Rev. Lett. **117**, 156403 (2016).

[27] J. P. Perdew and A. Zunger, Phys. Rev. B **23**, 5048 (1981).

[28] S. Groth, T. Dornheim, T. Sjostrom, F. D. Malone, W. M. C. Foulkes, and M. Bonitz, Phys. Rev. Lett. **119**, 135001 (2017).

[29] V. V. Karasiev, S. B. Trickey, and J. W. Dufty, Phys. Rev. B **99**, 195134 (2019).

[30] V. V. Karasiev, L. Calderín, and S. B. Trickey, Phys. Rev. E **93**, 063207 (2016).

[31] V. V. Karasiev, T. Sjostrom, and S. B. Trickey, Phys. Rev. E **86**, 056704 (2012).

[32] T. Sjostrom, F. E. Harris, and S. B. Trickey, Phys. Rev. B **85**, 045125 (2012).

[33] J. P. Perdew, K. Burke, and M. Ernzerhof, Phys. Rev. Lett. **77**, 3865 (1996).

[34] V. V. Karasiev, S. X. Hu, M. Zaghoo, and T. R. Boehly, Phys. Rev. B **99**, 214110 (2019).

[35] J. Heyd, J. E. Peralta, G. E. Scuseria, and R. L. Martin, J. Chem. Phys. **123**, 174101 (2005).

[36] J. P. Perdew, W. Yang, K. Burke, Z. Yang, E. K. U. Gross, M. Scheffler, G. E. Scuseria, T. M. Henderson, I. Y. Zhang, A. Ruzsinszky *et al.*, Proc. Natl. Acad. Sci. USA **114**, 2801 (2017).

[37] J. P. Perdew, M. Ernzerhof, and K. Burke, J. Chem. Phys. **105**, 9982 (1996).

[38] C. Adamo and V. Barone, J. Chem. Phys. **110**, 6158 (1999).

[39] J. Heyd, G. E. Scuseria, and M. Ernzerhof, J. Chem. Phys. **118**, 8207 (2003).

[40] A. D. Becke, J. Chem. Phys. **98**, 1372 (1993).

[41] M. Marsman, J. Paier, A. Stroppa, and G. Kresse, J. Phys.: Condens. Matter **20**, 064201 (2008).

[42] T. Baldsiefen, A. Cangi, and E. K. U. Gross, Phys. Rev. A **92**, 052514 (2015).

[43] T. Baldsiefen, A. Cangi, F. G. Eich, and E. K. U. Gross, Phys. Rev. A **96**, 062508 (2017).

[44] V. V. Karasiev, J. Chem. Phys. **118**, 8576 (2003).

[45] S. Ivanov, S. Hirata, and R. J. Bartlett, Phys. Rev. Lett. **83**, 5455 (1999).

[46] A. Görling, Phys. Rev. Lett. **83**, 5459 (1999).

[47] N. D. Mermin, Ann. Phys. (NY) **21**, 99 (1963).

[48] M. Greiner, P. Carrier, and A. Görling, Phys. Rev. B **81**, 155119 (2010).

[49] S. Pittalis, C. R. Proetto, A. Floris, A. Sanna, C. Bersier, K. Burke, and E. K. U. Gross, Phys. Rev. Lett. **107**, 163001 (2011).

[50] M. Levy, N. H. March, and N. C. Handy, *Many-Body Theory Of Molecules, Clusters, And Condensed Phases* (World Scientific, Singapore, 2010), pp. 542–545.

[51] D. Kang, K. Luo, K. Runge, V. V. Karasiev, and S. B. Trickey (unpublished).

[52] P. K. Patel, A. J. Mackinnon, M. H. Key, T. E. Cowan, M. E. Foord, M. Allen, D. F. Price, H. Ruhl, P. T. Springer, and R. Stephens, Phys. Rev. Lett. **91**, 125004 (2003).

[53] S. V. Faleev, M. van Schilfgaarde, T. Kotani, F. Léonard, and M. P. Desjarlais, Phys. Rev. B **74**, 033101 (2006).

[54] G. Kresse and J. Furthmüller, Phys. Rev. B **54**, 11169 (1996).

[55] G. Kresse and J. Furthmüller, Comput. Mater. Sci. **6**, 15 (1996).

[56] P. E. Blöchl, Phys. Rev. B **50**, 17953 (1994).

[57] G. Kresse and D. Joubert, Phys. Rev. B **59**, 1758 (1999).

[58] F. H. Allen, S. D. B. M. Bellard, M. D. Brice, B. R. X. A. N. A. Cartwright, A. Doubleday, H. Higgs, T. Hummelink, B. G. Hummelink-Peters, O. Kennard, and W. D. S. Motherwell, Acta Crystallogr., B: Struct. Cryst. Cryst. Chem. **35**, 2331 (1979).

[59] A. Maniopoulou, E. R. Davidson, R. Grau-Crespo, A. Walsh, I. J. Bush, C. R. A. Catlow, and S. M. Woodley, Comput. Phys. Commun. **183**, 1696 (2012).

[60] O. Greis, Y. Xu, T. Asano, and J. Petermann, Polymer **30**, 590 (1989).

[61] Y. Chatani, Y. Shimane, T. Inagaki, T. Ijitsu, T. Yukinari, and H. Shikuma, Polymer **34**, 1620 (1993).

[62] S. A. Saq'an, A. S. Ayesh, A. M. Zihlif, E. Martuscelli, and G. Ragosta, Polym. Test. **23**, 739 (2004).

[63] N. A. Lanzillo and C. M. Breneman, J. Phys.: Condens. Matter **28**, 325502 (2016).

[64] Y. Okada and Y. Tokumaru, J. Appl. Phys. **56**, 314 (1984).

[65] A. Schallamach, Proc. R. Soc. London, Ser. A **171**, 569 (1939).

[66] M. van Schilfgaarde, T. Kotani, and S. Faleev, Phys. Rev. Lett. **96**, 226402 (2006).

[67] A. J. Sabbah and D. M. Riffe, Phys. Rev. B **66**, 165217 (2002).

[68] L. Huang, J. P. Callan, E. N. Glezer, and E. Mazur, Phys. Rev. Lett. **80**, 185 (1998).

[69] R. Kubo, J. Phys. Soc. Jpn. **12**, 570 (1957).

[70] D. A. Greenwood, Proc. Phys. Soc. **71**, 585 (1958).